Successive Canard Explosions in a Singularly Perturbed Spruce-Budworm Model with Holling-II Functional Response*

Liyan Zhong[1] and Jianhe Shen[2,3,†]

Abstract By combining geometric singular perturbation theory (GSPT) with qualitative method, this paper analyzes the phenomenon of successive canard explosions in a singularly perturbed Spruce-Budworm model with Holling-II functional response. We select suitable parameters such that the critical curve is S-shaped, and the full model only admits a unique equilibrium. Then, under the variation of the breaking parameter, it is found that a canard explosion followed by an inverse canard explosion successively occurs in this model. That is, a relaxation oscillation arises via the first canard explosion, which persists for a large interval of parameter until it vanishes via the so-called inverse canard explosion. All these theoretical predictions are verified by numerical simulations.

Keywords Spruce-Budworm model, geometric singular perturbation theory, canard explosion, inverse canard explosion

MSC(2010) 34D23, 92B05, 34D40.

1. Introduction

The spruce budworm, also referred to as the spruce curling moth, is one of the most destructive insects in mixed spruce and fir forests in the eastern United States and Canada. According to available records in the United States and Canada, large outbreaks of budworm have occurred approximately every 40 years since the early 18th century, causing billions of dollars in forest damage each time [12, 30]. When the plague of insects occurs, the density of spruce budworm will suddenly increase hundreds of times in a few months, and it wreaks havoc on spruce and fir forests. Though only a few spruce and fir trees die in a disaster, it takes about seven to ten years for damaged trees to recover to their previous health [36]. Thus, the spruce

budworm, the spruce and fir forest evolve on different time scales. Therefore, the interaction between them would exhibit slow-fast nature. Hence, the dynamical model governing this process should be a singular perturbation problem.

In order to understand the interactions between the spruce budworm and its host, Ludwig, Jones and Holling [22] proposed the following three-dimensional spruce-budworm model

$$
\begin{aligned}
\frac{\mathrm{d}B}{\mathrm{d}t} &= r_B B \left(1 - \frac{B}{K_B} \right) - \beta \frac{B^2}{\alpha^2 + B^2}, \\
\frac{\mathrm{d}S}{\mathrm{d}t} &= r_S S \left(1 - \frac{S}{K_S} \times \frac{K_E}{E} \right), \\
\frac{dE}{dt} &= r_E E \left(1 - \frac{E}{K_E} \right) - P \frac{B}{S},
\end{aligned}
\tag{1.1}
$$

where B denotes the density of budworm, S is the total surface area of the branches in a stand, and E represents the condition of the foliage and health of the trees, which can be regarded as an "energy reserve". Additionally, K_S and K_E are the maximum values of S and E respectively, and K_B stands for the carrying capacity of B (see Ludwig for more details).

Since model (1.1) is three-dimensional, in general, its dynamical analysis is difficult. By ignoring the effect on "energy reserve" determining the condition of trees and foliage and retaining the essentials budworm and leaf area, May [24] simplified (1.1) to a two-dimensional one, namely,

$$
\begin{aligned}
\frac{dN}{dt} &= rN \left(1 - \frac{N}{kS} \right) - \beta \frac{PN^2}{\eta^2 S^2 + N^2}, \\
\frac{dS}{dt} &= \rho S \left(1 - \frac{S}{S_{\max}} \right) - \delta N,
\end{aligned}
\tag{1.2}
$$

in which N is the population density of the larvae, S is the average leaf area of the spruce, r and ρ describe the intrinsic growth rates of the budworm and the leaves respectively, kS and S_{max} represent the carrying capacity of budworm population and spruce leaf area respectively, k measures the degree that leaves can accommodate the larvae, β is the coefficient of proportionality, and the term

$$
\beta \frac{PN^2}{\eta^2 S^2 + N^2}
$$

describes the predation pressure on budworm population by parasitoids, insectivorous birds, etc. For more biological motivations about (1.2), one can refer to [24]. From model (1.2), it can be noted that the carrying capacity of the budworm population and the Holling-III functional response function now depend on S, i.e. the density of the spruce, and the predation from the budworm to the spruce is assumed to be linearly dependent on N. Under these assumptions, the original three-dimensional model (1.1) is changed to the two-dimensional one (1.2). This dimension reduction is mainly biological rather than mathematical ways like the center manifold reduction, etc.

In May [24], it was assumed that $\rho \ll r$, i.e., the intrinsic growth rates of the budworm and of the leaves are of different orders. Under this condition, model (1.2) can be rewritten into the form of singular perturbation problems. Hence, it can be

analyzed under the framework of GSPT. Rasmusse, Wyller and Vik [28] investigated the existence of relaxation oscillation in the singular perturbation version of model (1.2) by applying GSPT. By taking the effects of delay and diffusion into account, the delayed and reaction-diffusion versions of model (1.2) have also been studied in [38] and [15] respectively. In fact, bifurcations in various predator-prey systems under singular or regular perturbation have been studied extensively (see e.g., [26, 33, 39].

Recently, Tai and Zhang [34] have proposed a more general spruce-budworm model, namely,

$$
\begin{aligned}
\frac{dN}{dt} &= rN\left(1 - \frac{N}{\kappa S}\right) - \beta\frac{PN^2}{\eta^2 S^2 + N^2}, \\
\frac{dS}{dt} &= \rho S\left(1 - \frac{S}{S_{\max}}\right) - \frac{\delta S}{K + S}N,
\end{aligned}
\tag{1.3}
$$

where the Holling's type II functional response

$$
\frac{\delta S}{K + S}N
$$

is introduced to replace the linear predation δN in the second equation of model (1.2).

After rescaling

$$
x = \frac{N}{\kappa S}, \quad y = \frac{r\kappa S}{\beta P}, \quad z = xy = \frac{rN}{\beta P}, \quad \tau = \rho t
$$

on variables, and denoting

$$
\varepsilon = \frac{\rho}{r}, \quad \alpha = \frac{\eta}{\kappa}, \quad e = \frac{\delta\kappa}{\rho}, \quad d = \frac{r\kappa S_{\max}}{\beta P}, \quad A = \frac{r\kappa K}{\beta P},
$$

system (1.3) can be changed to

$$
\begin{aligned}
\varepsilon\frac{dx}{d\tau} &= f_0\left(x, y; \alpha^2\right) - \varepsilon x g_0\left(x, y; e, d, A\right), \\
\frac{dy}{d\tau} &= y g_0\left(x, y; e, d, A\right)
\end{aligned}
\tag{1.4}
$$

with

$$
\begin{aligned}
f_0\left(x, y; \alpha^2\right) &= x(1 - x) - \frac{1}{y}\frac{x^2}{x^2 + \alpha^2}, \\
g_0\left(x, y; e, d, A\right) &= 1 - \frac{y}{d} - \frac{exy}{A + y},
\end{aligned}
$$

where it is assumed that

$$
0 < \varepsilon = \frac{\rho}{r} \ll 1, x \geq 0, y > 0.
$$

Obviously, model (1.4) is a two-dimensional singular perturbation system with the slow variable y and the fast variable x. In Tai and Zhang [34], the authors constructed an asymptotic approximation to the relaxation oscillation of model (1.4) by gluing the outer and inner solutions. Also, Tai and Zhang [34] gave an asymptotic expression of the period of relaxation oscillation.

In this article, based on the work of Tai and Zhang [34], we further pay attention to the mechanisms governing the birth and disappearance of relaxation oscillation in model (1.4) by using GSPT [11, 13, 14]. That is, we are concerned with the phenomenon of successive canard explosions in model (1.4) via a geometrical point of view. In fact, if the unique equilibrium is moved from the repelling branch to the attracting one or vice versa via the extreme points, then the canard explosion followed by the inverse canard explosion occurs, leading to the birth and the disappearance of relaxation oscillations.

So far, it has been well-known that canard explosion is a phenomenon describing a transition from a small amplitude limit cycle to a large amplitude relaxation, which occurs in a very narrow parameter range. Krupa and Szmolyan [16] proposed a dynamical system-based method, namely, a blow-up technique to detect the birth of canard explosion and relaxation oscillations in singular perturbation planar vector fields, where the Hopf and canard curves were explicitly determined. Qin et al., [27] further studied the degenerate canard explosion in singular perturbation Liénard equation and gave the higher-order approximation to the associated canard curve. Now, the theoretical results on canard phenomenon are called canard theory [9, 16, 19, 20]. After transforming a singular perturbation model into its associated normal form, canard theory has been found applications in a variety of physical, chemical and biological models (see e.g., [2–7, 18, 23, 25, 27, 29, 31, 32, 35]). Under the assumption that model (1.4) admits only a unique positive equilibrium, this article is devoted to revealing the birth and the disappearance of canard explosions as well as the associated relaxation oscillations by using GSPT and canard theory. That is, two successive canard explosions occurring in model (1.4) are detected in this article. The main conclusions obtained in the present paper are as follows.

(A) If the unique positive equilibrium is located at the repelling or attracting branches of the critical curve, then it is either globally stable or unstable with a limit cycle surrounding it.

(B) If the unique positive equilibrium moves from the attracting to the repelling branch or vice versa via the extreme points, then canard explosion or inverse canard explosion occurs accompanying with the birth or the disappearance of relaxation oscillations. That is, two successive canard explosions occur in (1.4) continuously.

The article is organized as follows. In Section 2, we determine the number, types and stability of positive equilibria of system (1.4). In Section 3, the limiting slow and fast dynamics of model (1.4) are separated under the assumption that model (1.4) admits only a unique positive equilibrium. Section 4 gives the main results of this article. First, we prove that the unique positive equilibrium is globally stable or unstable with a limit cycle surrounding it. Then, by using GSPT and canard theory, the occurrence of a canard explosion followed by an inverse canard explosion, and accompanying with the birth and the disappearance of relaxation oscillations are revealed. All the theoretical predictions are verified and visualized through numerical simulations. Finally, the biological motivations and interpretations on the study in this article are given in Section 5.

2. The number and types of positive equilibria

The number, positions and types of positive equilibria greatly affect the slow and fast dynamics of model (1.4), including the birth and disappearance of canard explosions and relaxation oscillations. Therefore, first of all, we determine the number, positions and types of positive equilibria.

2.1. The number of positive equilibria

Obviously, $(x_0, y_0) = (0, d)$ is always a boundary equilibria of model (1.4). The positive equilibrium of (1.4) are governed by

$$
\begin{aligned}
x(1-x) - \frac{1}{y}\frac{x^2}{x^2+\alpha^2} &= 0, \\
1 - \frac{y}{d} - \frac{exy}{A+y} &= 0.
\end{aligned}
\tag{2.1}
$$

From the first equation of (2.1), one obtains

$$
y = \varphi(x) = \frac{x}{(x^2+\alpha^2)(1-x)}.
\tag{2.2}
$$

Since $x > 0$ and $y > 0$, all the possible positive equilibria denoted by $E(x_*, y_*)$ are restricted in this strip as follows

$$
S_0 = \{(x, y) \mid 0 < x < 1, y > 0\}.
$$

By the second equation of (2.1), we get

$$
x = w(y) = \frac{1}{e}\left(1 - \frac{A+y}{d} + \frac{A}{y}\right).
\tag{2.3}
$$

It can be verified that

$$
w'(y) = \frac{1}{e}\left(-\frac{1}{d} - \frac{A}{y^2}\right) < 0.
\tag{2.4}
$$

Therefore, the inverse function $w^{-1}(x)$ exists with

$$
\left(w^{-1}\right)'(x) = \frac{1}{w'(y)} < 0
\tag{2.5}
$$

and

$$
w''(y) = \frac{2A}{ey^3} > 0.
$$

Consequently, $x = w(y)$ is decreasing monotonously and concave upward in the x-y plane.

Moreover, it can be noted that $\varphi(0) = 0$, $\lim_{x \to 1^-} \varphi(x) = +\infty$, $w(d) = 0$, $\lim_{y \to 0^+} w(y) = +\infty$. Thus, we can deduce that at least there exists an intersection point in the region S_0 for the two nullclines associated with model (1.4). In other words, system (1.4) admits at least one positive equilibrium.

To determine the number of positive equilibria, we turn to analyze the shape of the curve $y = \varphi(x)$. Differentiating it with respect to x yields

$$
\varphi'(x) = \frac{p(x)}{(x^2+\alpha^2)^2(1-x)^2},
\tag{2.6}
$$

where
$$p(x) = 2x^3 - x^2 + \alpha^2. \tag{2.7}$$

Denoting $y = p(x)$, there is no doubt that it has a unique maximal extreme point at $x = 0$ and a unique minimal extreme point at $x = \frac{1}{3}$.

Let $\Delta = \frac{\alpha^2}{16}\left(\alpha^2 - \frac{1}{27}\right)$, and take x, y in the region S_0. Then we have the following arguments.

(I_1) If $\alpha^2 > \frac{1}{27}$, then $y = p(x)$ has no zero in the interval $(0,1)$ and $p(x) > 0$, which implies that $y = \varphi(x)$ is monotonically increasing in S_0.

(I_2) If $\alpha^2 = \frac{1}{27}$, then $y = p(x)$ has a unique zero $x = \frac{1}{3}$ in the interval $(0,1)$ and $p(x) \geq 0$, and it indicates that $y = \varphi(x)$ is monotonically increasing in S_0 and has a unique critical point at $x = \frac{1}{3}$.

(I_3) If $0 < \alpha^2 < \frac{1}{27}$, then $y = p(x)$ has two zeros, denoted respectively by x_1 and x_2 with $0 < x_1 < \frac{1}{3} < x_2 < \frac{1}{2} < 1$. When $x_1 < x < x_2$, $x = x_1$ or $x = x_2$ and, $0 < x < x_1$ or $x_2 < x < \frac{1}{2}$, we respectively have $p(x) < 0$, $p(x) = 0$ and $p(x) > 0$. This means that $y = \varphi(x)$ decreases and increases monotonically, when $x_1 < x < x_2$ and $0 < x < x_1$ or $x_2 < x < \frac{1}{2}$ respectively. The function $y = \varphi(x)$ admits a maximal extreme point at $x = x_1$ and a minimal extreme point at $x = x_2$.

Corresponding to the above three cases, the graphs of $y = p(x)$ and $y = \varphi(x)$ are respectively plotted in Figure 1(a) and (d), Figure 1(b) and (e), and Figure 1(c) and (f).
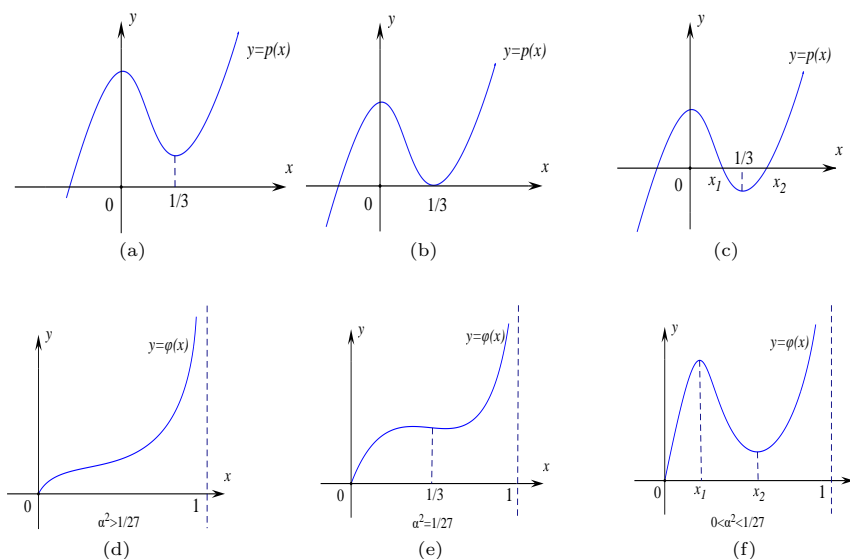

Figure 1. Sketch plots of the curves $y = p(x)$ and $y = \varphi(x)$, when $\alpha^2 > 1/27$, $\alpha^2 = 1/27$ and $0 < \alpha^2 < 1/27$ respectively.

Proposition 2.1 *For system (1.4), when x, y are in the strip S_0, the following statements hold.*

(A) If $\alpha^2 \geq \frac{1}{27}$, then (1.4) has a unique positive equilibra.

(B) If $0 < \alpha^2 < \frac{1}{27}$, then (1.4) has possibly one, two or three positive equilibriums.

Proof. The proof of Proposition 2.1 can be obtained by following from the number of intersections between the curves defined by (2.2) and (2.3), which can be seen easily from the previous analysis (also see Figure 2). We omit the details here. $\square$
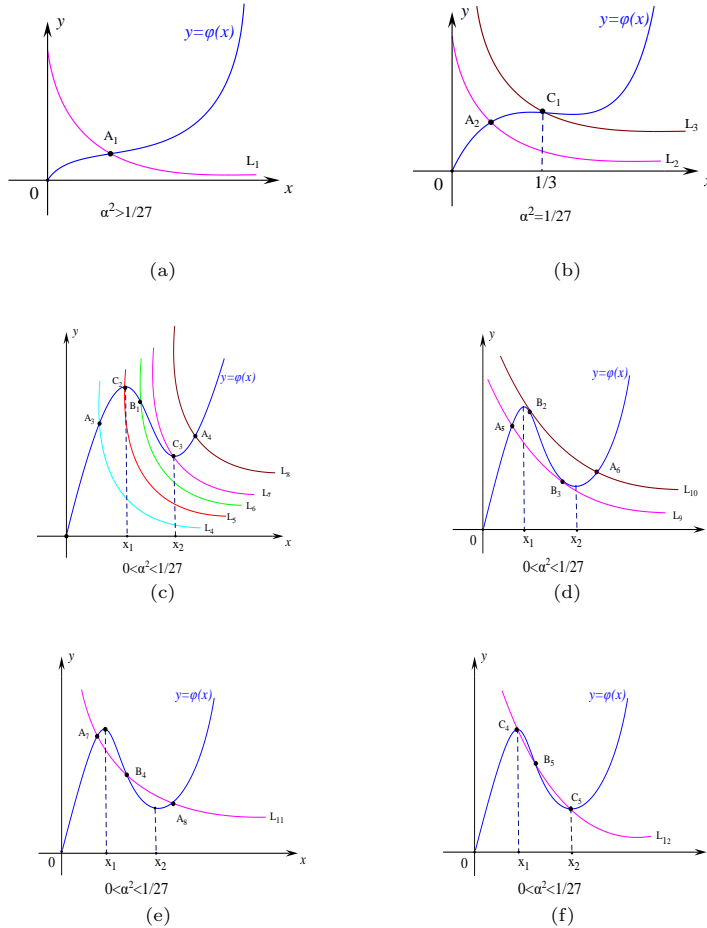

Figure 2. The intersections between $x = w(y)$ and $y = \varphi(x)$ in different situations, in which $L_i, i = 1, 2, \cdots, 12$ represents the curve $x = w(y)$, and $A_i, i = 1, 2, \cdots, 8$, $B_i, i = 1, 2, \cdots, 5$ and $C_i, i = 1, 2, \cdots, 5$ stand for the positive equilibria.

Remark 2.1. When model (1.4) admits two positive equilibria, then the curves φ and w^{-1} are tangential at one of the intersections (see Figure 2(d) for a geometric illustration where L_9 and L_{10} are tangential at one of the equilibria). Obviously, this case is a critical situation.

2.2. The types of positive equilibria

Proposition 2.2. *Denote $E(x_*, y_*)$ a positive equilibrium of system (1.4). $E(x_*, y_*)$ can be a node, a focus (strong or weak), a saddle or a degenerate equilibrium.*

Proof.   The Jacobian matrix of system (1.4) is

$$J = \begin{pmatrix} \frac{1}{\varepsilon}\frac{\partial f_0}{\partial x} - g_0 - x\frac{\partial g_0}{\partial x} & \frac{1}{\varepsilon}\frac{\partial f_0}{\partial y} - x\frac{\partial g_0}{\partial y} \\ y\frac{\partial g_0}{\partial x} & g_0 + y\frac{\partial g_0}{\partial y} \end{pmatrix},$$

where

$$\frac{\partial f_0}{\partial x} = 1 - 2x - \frac{1}{y}\frac{2\alpha^2 x}{(x^2+\alpha^2)^2}, \quad \frac{\partial f_0}{\partial y} = \frac{1}{y^2}\frac{x^2}{x^2+\alpha^2}, \quad \frac{\partial g_0}{\partial x} = -\frac{ey}{A+y}, \quad \frac{\partial g_0}{\partial y} = -\frac{1}{d} - \frac{eAx}{(A+y)^2}.$$

The trace and determinant of J evaluated at $E(x_*, y_*)$ are respectively

$$\text{tr}(J) = -\frac{1}{\varepsilon}\frac{p(x_*)}{x_*^2+\alpha^2} + 1 - \frac{2y_*}{d} - \frac{eAx_*y_*}{(A+y_*)^2} \tag{2.8}$$

and

$$\det(J) = \frac{1}{\varepsilon}\left(\frac{p(x_*)}{x_*^2+\alpha^2}\left(\frac{y_*}{d} + \frac{eAx_*y_*}{(A+y_*)^2} \right) + \frac{ex_*^2}{(A+y_*)(x_*^2+\alpha^2)} \right). \tag{2.9}$$

Since $E(x_*, y_*)$ satisfies (2.1),

$$\frac{ex_*y_*}{A+y_*} = 1 - \frac{y_*}{d}, \quad x_* = y_*\left(x_*^2+\alpha^2\right)(1-x_*). \tag{2.10}$$

By substituting (2.10) into (2.9) and taking (2.4), (2.5) and (2.6) into account, after simplification, we have

$$\det(J)$$
$$= \frac{1}{\varepsilon}\left(\left(x_*^2+\alpha^2\right)\left(1-x_*^2\right)\varphi'(x_*)\left(\frac{y_*}{d} + \frac{A}{A+y_*}\left(1-\frac{y_*}{d}\right) \right) + \frac{ey_*^2\left(x_x^2+\alpha^2\right)(1-x_*)^2}{A+y_*} \right)$$
$$= \frac{\left(x_*^2+\alpha^2\right)(1-x_*)^2\left(y_*^2+Ad\right)}{\varepsilon d(A+y_*)}\left(\varphi'(x_*) + \frac{e}{\frac{1}{d}+\frac{A}{y_*^2}} \right)$$
$$= \frac{\left(x_*^2+\alpha^2\right)(1-x_*)^2\left(y_*^2+Ad\right)}{\varepsilon d(A+y_*)}\left(\varphi'(x_*) - \omega^{-1}(x_*) \right). \tag{2.11}$$

Keeping in mind that ε is small enough, it can be concluded that

(A) For any α, if $p(x_*) > 0$, that is, the equilibrium $E(x_*, y_*)$ is located on the increasing parts of the curve $y = \varphi(x)$ (see the points $E = A_i, i = 1, 2, \cdots, 8$ in Figure 2). In this situation, one follows from (2.8) and (2.9) that $\text{tr}(J) < 0$ and $\det(J) > 0$. Thus, E is a stable focus or node.

(B) For $0 < \alpha^2 < \frac{1}{27}$, if $p(x_*) < 0$, that is, the equilibrium $E(x_*, y_*)$ is located on the decreasing parts of the curve $y = \varphi(x)$ denoted by $I_m = \{(x,y)|x_1 < x < x_2, y = \varphi(x)\}$, then the followings hold.

    (b_1) When model (1.4) admits only a unique positive equilibrium (see, e.g., $E = B_1$ in Figure 2(c)), in this case, we have $(w^{-1})'(x_*) < \varphi'(x_*) < 0$. Thus, it follows from $\text{tr}(J) > 0$ and $\det(J) > 0$ that E is an unstable focus or node.

(b_2) When model (1.4) admits two positive equilibria (see, e.g., $E = B_2$ and $E = B_3$ shown in Figure 2(d)), in this case, one gets $(w^{-1})'(x_*) = \varphi'(x_*)$. Then, it follows from (2.8) and (2.11) that $\det(J) = 0$ that E is a degenerate equilibrium.

(b_3) When model (1.4) admits three positive equilibria (see, e.g., $E = B_4$ and $E = B_5$ in Figure 2(e) and (f)), in this case, we have $\varphi'(x_*) < (w^{-1})'(x_*) < 0$. Thus, by (2.8) and (2.11), it follows that $\det(J) < 0$. Therefore, in this case, E is a saddle.

(C) For any α, if $p(x_*) = 0$, in this case, it means that the equilibrium E exactly coincides with the critical points of the curve $y = \varphi(x)$ (see, e.g., $E = C_i, i = 1, 2, \cdots, 5$, in Figure 2(b), (c) and (f)). Then, it follows from (2.8) and (2.9) that $\det(J) > 0$ and

$$\operatorname{tr}(J) = \frac{d\left(A + y_*\right)^2 - 2y_*\left(A + y_*\right)^2 - edAx_*y_*}{d\left(A + y_*\right)^2}.$$

Denoting $C_* = d\left(A + y_*\right)^2 - 2y_*\left(A + y_*\right)^2 - edAx_*y_*$, we have

(c_1) if $C_* > 0$, then $\operatorname{tr}(J) > 0$, thus E is an unstable focus or node;

(c_2) if $C_* < 0$, then $\operatorname{tr}(J) < 0$, thus E is a stable focus or node;

(c_3) if $C_* = 0$, then $\operatorname{tr}(J) = 0$. Since E satisfies (2.3), $d = \frac{y_*(A+y_*)}{A+y_*-ex_*y_*}$ which gives $e = \frac{(A+x_*)^2}{(A+2y)x_*y_*}$ after calculation, thus E is a weak focus or center.

The proof of Proposition 2.2 is finished.   □

3. The limiting slow and fast dynamics associated with model (1.4)

By $\varepsilon = \tau/\bar{s}$, one gets the fast system associated with system (1.4), namely,

$$\begin{aligned}
\varepsilon\frac{dx}{d\bar{s}} &= f_0\left(x, y; \alpha^2\right) - \varepsilon x g_0\left(x, y; e, d, A\right), \\
\frac{dy}{d\bar{s}} &= \varepsilon y g_0\left(x, y; e, d, A\right).
\end{aligned} \tag{3.1}$$

More concisely, the slow and fast systems are respectively

$$\begin{aligned}
\varepsilon\dot{x} = \varepsilon\frac{dx}{d\tau} &= x(1-x) - \frac{x^2}{y\left(x^2 + \alpha^2\right)} - \varepsilon x\left(1 - \frac{y}{d} - \frac{exy}{A+y}\right) = f(x, y; \varepsilon, \eta), \\
\dot{y} = \frac{dy}{d\tau} &= y\left(1 - \frac{y}{d} - \frac{exy}{A+y}\right) = g(x, y; \varepsilon, \eta)
\end{aligned} \tag{3.2}$$

and

$$\begin{aligned}
x' = \frac{dx}{d\bar{s}} &= x(1-x) - \frac{x^2}{y\left(x^2 + \alpha^2\right)} - \varepsilon x\left(1 - \frac{y}{d} - \frac{exy}{A+y}\right) = f(x, y; \varepsilon, \eta), \\
y' = \frac{dy}{d\bar{s}} &= \varepsilon y\left(1 - \frac{y}{d} - \frac{exy}{A+y}\right) = \varepsilon g(x, y; \varepsilon, \eta),
\end{aligned} \tag{3.3}$$

where $\eta = (\alpha^2, e, A, d)$. Taking $\varepsilon \to 0$, one obtains the reduced system

$$
\begin{aligned}
0 &= x(1-x) - \frac{x^2}{y\left(x^2 + \alpha^2\right)}, \\
\dot{y} &= y\left(1 - \frac{y}{d} - \frac{exy}{A+y}\right)
\end{aligned}
\tag{3.4}
$$

and the layer system

$$
\begin{aligned}
x' &= x(1-x) - \frac{x^2}{y\left(x^2 + \alpha^2\right)}, \\
y' &= 0,
\end{aligned}
\tag{3.5}
$$

where the critical curves are

$$
C_0 = \left\{ (x,y) \mid x = 0 \ or \ y = \varphi(x) = \frac{x}{\left(x^2 + \alpha^2\right)\left(1 - x\right)} \right\}.
$$

The curve of $y = \varphi(x)$ has three topologically different shapes (see Figure 1(d), (e) and (f)). Hereinafter, we always assume that $y = \varphi(x)$ is S-shaped, i.e., we always set $0 < \alpha^2 < \frac{1}{27}$ such that the critical curve consists of

$$
M_0 = \{(x,y) \mid y = \varphi(x)\} = M_0^l \cup E_1 \cup M_0^m \cup E_2 \cup M_0^r
$$

with

$$
\begin{aligned}
M_0^l &= \left\{ (x,y) \mid 0 < x < x_1, 0 < y < \varphi(x_1) \right\}, \\
M_0^m &= \left\{ (x,y) \mid x_1 < x < x_2, \varphi(x_1) < y < \varphi(x_2) \right\}, \\
M_0^r &= \left\{ (x,y) \mid x_2 < x < 1, y > \varphi(x_2) \right\},
\end{aligned}
$$

and $E_1\left(x_1, y_1\right)$ and $E_2\left(x_2, y_2\right)$ are respectively the maximal and minimal extreme points (see, e.g., Figure 1(f)).

If $(x,y) \in M_0^l \cup M_0^r$, then $\varphi'(x) > 0$. If $(x,y) \in M_0^m$, then $\varphi'(x) < 0$, and if $(x,y) = E_1 \ or \ E_2$, then $\varphi'(x) = 0$. Thus, by geometric singular perturbation theory, M_0^l and M_0^r are normally hyperbolic attracting, M_0^m is normally hyperbolic repelling, and E_1 and E_2 are two generic fold points.

In addition, when system (1.4) admits only a unique positive equilibrium, one can see that, if $x < w(y)$, then $\dot{y} > 0$; if $x > w(y)$, then $\dot{y} < 0$. Thus, along the critical curve $x = 0$, the slow flows are downward for $y > d$ and upward for $y < d$, and along the critical curve $y = \varphi(x)$, the slow flows are upward for $x < w(y)$ and downward for $x > w(y)$.

After the limiting slow-fast flows have been separated, we obtain the singular orbits shown in Figure 3, where the unique equilibrium is situated at different positions.

4. Canard and inverse canard explosions in model (1.4)

Based on the preliminary analysis given in the previous section, in Section 4, we are devoted to studying the slow and fast dynamics including the successive births of canard explosion and inverse canard explosion in model (1.4) (equivalently, (3.2)/(3.3)).

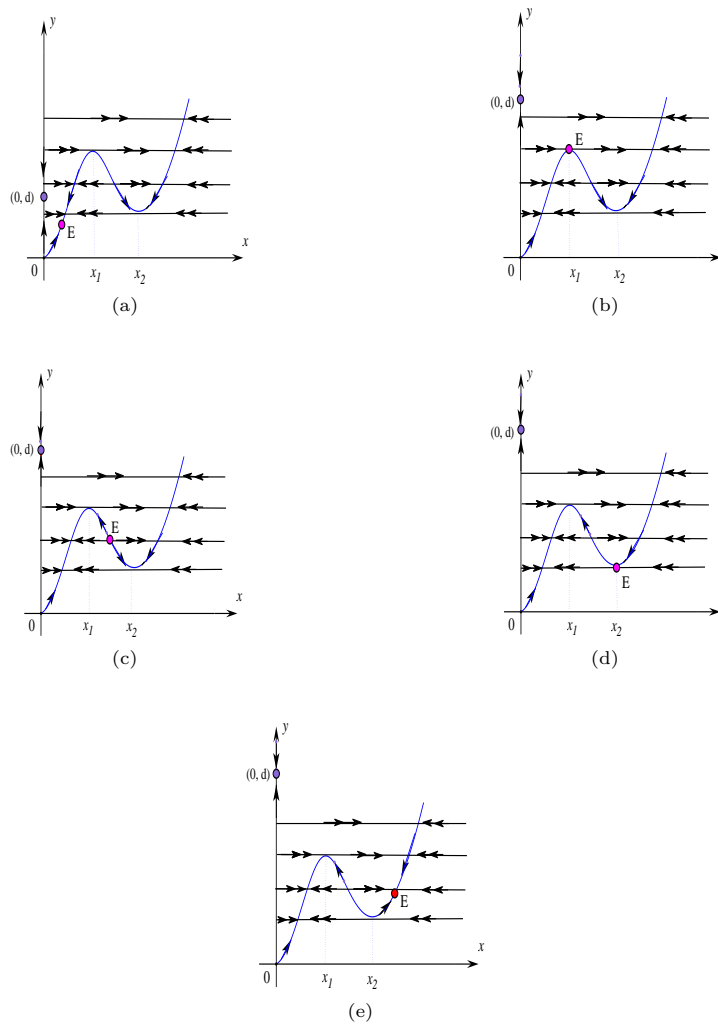For simplicity, we make the following assumptions:

Figure 3. The limiting slow and fast dynamics associated with model (1.4). In the figures, the orbits marked with double arrows and single arrow represent respectively the fast and slow flows.

(H_1) $0 < \varepsilon \ll 1$;

(H_2) system (3.3) admits a unique positive equilibrium, denoted by $E(x_*, y_*)$;

(H_3) the critical curve $y = \varphi(x)$ is S-shaped (implying that $0 < \alpha^2 < \frac{1}{27}$) with two contact points $E_1(x_1, y_1)$ and $E_2(x_2, y_2)$.

Remark 4.1. It is worth reminding that when

$$d_1 = \frac{y_1(A + y_1)}{A + y_1 - ex_1y_1} \text{ (andrespectively, } d_2 = \frac{y_2(A + y_2)}{A + y_2 - ex_2y_2}),$$

it can be verified that

$$E(x_*, y_*) = E_1(x_1, y_1) \text{ (respectively, } E(x_*, y_*) = E_2(x_2, y_2)).$$

That is, along this critical parameter value, the unique positive equilibrium coincides with the contact point.

Theorem 4.1. *Under the assumptions* (H_1)-(H_3), *the following statements hold.*

(A) *For* $E \neq E_1$ *or* E_2, *the equilibrium* E *is either globally stable, or unstable with a limit cycle surrounding it.*

(B) *When the parameter* d *varies from* d_1 *to* d_2, *system (3.3) possesses continuously a canard explosion, and then a relaxation oscillation followed by an inverse canard explosion after which the relaxation oscillation disappears, where* d_1 *and* d_2 *are defined in Remark 4.1.*

Before carrying out the proof of Theorem 4.1, we provide the following lemma first.

Lemma 4.1. *For system (3.3), with* ε *sufficiently small, the set*

$$Q = \{(x,y) \mid 0 \leqslant x < 1, \quad y > 0\}$$

is positively invariant, that is, all the orbits of system (3.3) in the first quadrant have their ω-*limits inside the region* Q *(see Figure 4).*

Proof.   Obviously, $x = 0$ is an invariant line. Restricting the first equation of (3.3) on $x = 1$ yields

$$\left.\frac{dx}{d\bar{s}}\right|_{x=1} = -\frac{1}{y(1+\alpha^2)} - \varepsilon\left(1 - \frac{y}{d} - \frac{ey}{A+y}\right) < 0,$$

where ε small enough and $y > 0$ have been taken into account. Restricting the second equation of (3.3) on $y = d$ and $y = d + c$ ($c > 0$) respectively yield

$$\left.\frac{dy}{d\bar{s}}\right|_{y=d} = -\varepsilon d\frac{exd}{A+d} < 0,$$

and

$$\left.\frac{dy}{d\bar{s}}\right|_{y=d+c} = \varepsilon(d+c)\left(1 - \frac{d+c}{d} - \frac{ex(d+c)}{A+d+c}\right) < 0,$$

for $0 < x < 1$. Thus, the set Q is positively invariant (see Figure 4).

$\square$

4.1. Proof of Theorem 4.1 (A)

(I_1) For $E \in M_0^l$ *or* M_0^r, we prove that E is globally stable. Note that all the possible positive equilibria are located in the strip $S_0 = \{(x,y) \mid 0 < x < 1, y > 0\}$ and the critical curve $y = \varphi(x)$ satisfying $\varphi(0) = 0$, $\lim\limits_{x\to 1^-} \varphi(x) = +\infty$ as analysed previously. To obtain our goal, we divide the first quadrant into three parts, namely,

$$S_0^l = \{(x,y) \mid 0 < x < x_1, y > 0\},$$

$$S_0^m = \{(x,y) \mid x_1 < x < x_2, y > 0\}$$
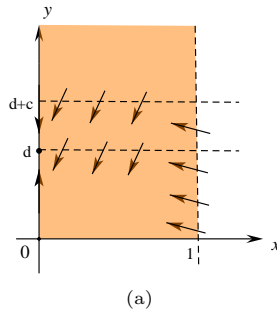
and

$$S_0^r = \{(x,y) \mid x > x_2, y > 0\}.$$

(a)

Figure 4. The positively invariant region of system (3.3).

Constructing the following Dulac function

$$D(x, y) = x^{-2}yd\left(x^2 + \alpha^2\right)(A + y),$$

it can be verified that

$$\frac{\partial f(x, y; \varepsilon, \eta)D(x, y)}{\partial x}$$
$$= -\varepsilon y\left(\left(1 - \alpha^2 x^{-2}\right)(d(A + y) - y(A + y) - exyd) - edy\left(x + \alpha^2 x^{-2}\right)\right)$$
$$\quad - dy(A + y)x^{-2}\left(2x^3 - x^2 + \alpha^2\right),$$

and

$$\frac{\partial g(x, y; \varepsilon, \eta)D(x, y)}{\partial y} = \varepsilon\left(x + \alpha^2 x^{-2}\right)\left(2y((A + y)(d - y) - exyd) + y^2(d - A - 2y - exd)\right).$$

Clearly, when $0 < \alpha^2 < \frac{1}{27}$, we have $2x^3 - x^2 + \alpha^2 > 0$ in the region S_0^l or S_0^r. It follows that, for ε is small enough, one gets in S_0^l or S_0^r that

$$\frac{\partial f(x, y; \varepsilon, \eta)D(x, y)}{\partial x} + \frac{\partial g(x, y; \varepsilon, \eta)D(x, y)}{\partial y} < 0.$$

Thus, by Dulac's criterion, no closed orbit can lie entirely in the region S_0^l or S_0^r. It is also impossible that an closed orbit lies entirely in the region S_0^m since E is located at one of the attracting branches.

By the slow-fast analysis given in Section 3, for $E \in M_0^l \cup M_0^r$, the unique equilibrium is hyperbolic and stable. Thus, by combining with Lemma 4.1, we can conclude that E is globally stable in the first quadrant. This ends the proof.

Next, we give numerical simulations to illustrate this conclusion (see Figures 5 and 6). In these figures, we set $\varepsilon = 0.0005$, $\alpha^2 = 0.008$, $A = 10$ and $e = 3.363388515$ such that system (3.3) has two contact points $E_1(0.1000000000, 6.172839506)$ and $E_2(0.4828427125, 3.871854472)$.

(i_1) We take $d = 10.08197866$ such that (3.3) has a unique positive equilibrium $E(0.6064936519, 4.100887120) \in M_0^r$. In this case, numerical simulations are shown in Figure 5. More precisely, in Figure 5(a), the green, magenta, blue and coral curves represent respectively the orbits starting from $(0.01, 4)$, $(0.25, 4.5)$, $(0.3, 5)$ and $(0.9, 4.5)$. In Figure 5(b), the magenta and coral curves

respectively represent the time histories of the predator $x(t)$ and the prey $y(t)$ with $x(0) = 0.04$ and $y(0) = 5$. All the orbits approach to the equilibrium $E(0.6064936519, 4.100887120) \in M_0^r$, as time goes to infinity.

(i_2) We take $d = 5.581978656$ such that (3.3) has a unique positive equilibrium $E(0.05407801131, 5.233190604) \in M_0^l$. In this case, numerical simulations are shown in Figure 6. More precisely, in Figure 6(a), the magenta, coral, green, blue and red curves represent respectively the orbits starting from points $(0.3,6.5)$, $(0.9, 4.5)$, $(0.25, 4.1)$, $(0.05, 4.4)$ and $(0.01, 6)$. In Figure 6(b), the magenta and coral curves respectively represent the time histories of the predator $x(t)$ and the prey $y(t)$ with $x(0) = 0.7$ and $y(0) = 4.5$. All the orbits approach to the equilibrium $E(0.05407801131, 5.233190604) \in M_0^l$, as time goes to infinity.
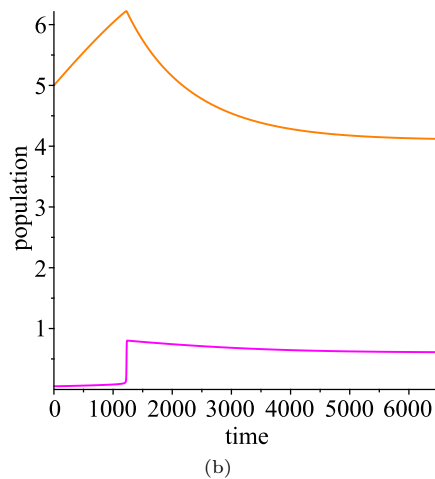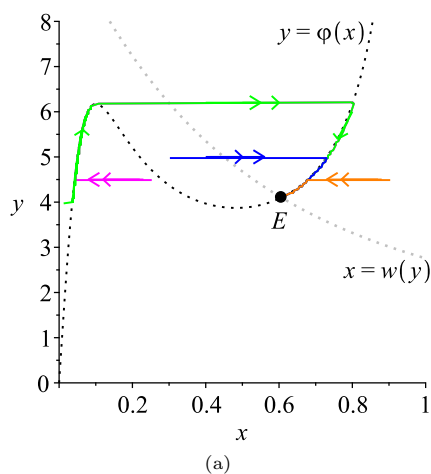

Figure 5. (a) The unique equilibrium $E \in M_0^r$ is a global attractor of system (3.3); (b) The time histories of the prey and the predator.

(I_2) For $E \in M_0^m$, we prove that E is unstable with a limit cycle surrounding it.

$y = \varphi(x)$

$x = w(y)$

E
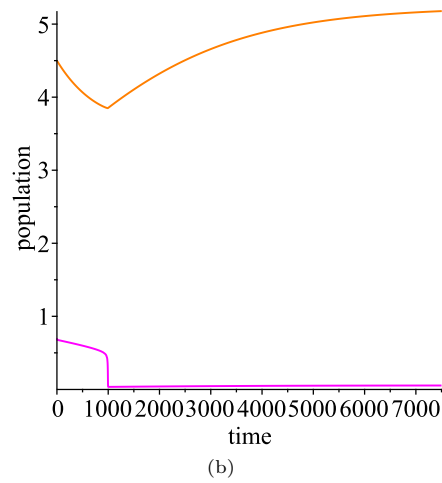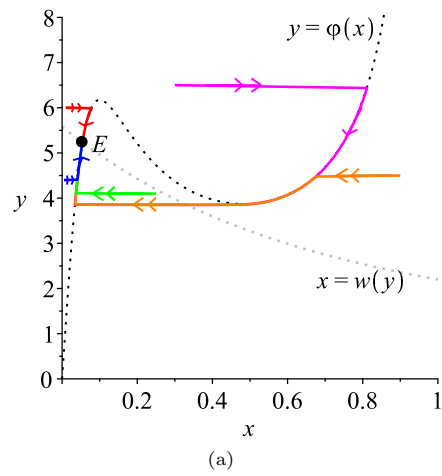
y

x

(a)

population

time

(b)

Figure 6. (a) The unique equilibrium $E \in M_0^l$ is a global attractor of system (3.3); (b) The time histories of the prey and the predator.

By Lemma 4.1, we have known that Q is positively invariant, and all orbits in the first quadrant have their ω limits inside it. In addition, by following the case $B(b_1)$ in Proposition 2.2 which has been illustrated that E is unstable when $0 < \alpha^2 < \frac{1}{27}$ and $p(x_*) < 0$, which is equivalent to $E \in M_0^m$. Therefore, the conclusion follows directly from Poincaré Annular Region Theorem [21] (also see the related articles [1, 8, 10, 37]).

A numerical example for the existence of limit cycle is given in Figure 7. As before, we set $\varepsilon = 0.0005$ and $\alpha^2 = 0.008$ such that (3.3) has two contact points $E_1(0.1000000000, 6.172839506)$ and $E_2(0.4828427125, 3.871854472)$. We take $A = 16$, $e = 15$ and $d = 30.59887166$, then (3.3) admits a unique positive equilibrium $E(0.2450292459, 4.770103015)$. The initial value of the orbit is chosen arbitrarily $x(0) = 0.25, y(0) = 4.2$.
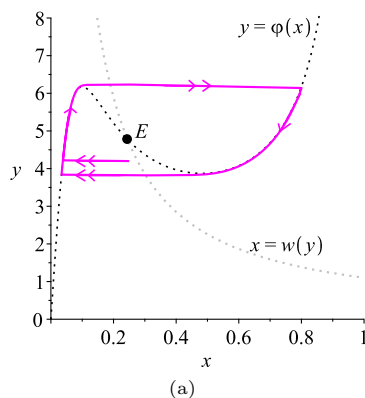

Figure 7. A limit cycle (relaxation oscillation) surrounding E, when $E \in M_0^m$.

4.2. Proof of Theorem 4.1(B)

When $E = E_1$ (respectively $E = E_2$), i.e., $(x_*, y_*) = (x_1, y_1)$ (respectively $(x_*, y_*) = (x_2, y_2)$), for this situation, by (2.3), we have

$$d = d_* = \frac{y_* (A + y_*)}{A + y_* - ex_*y_*},$$

where $* = 1, 2$.

In this case, it can be verified that

$$f(x_*, y_*, 0, \eta_*) = 0, \qquad f_x(x_*, y_*, 0, \eta_*) = 0, \qquad g_x(x_*, y_*, 0, \eta_*) = 0,$$
$$f_{xx}(x_*, y_*, 0, \eta_*) = 2\left(1 - x_*^2(2x_* - 1)\right) > 0 \text{ (since } 0 < x_* < 1),$$
$$f_y(x_*, y_*, 0, \eta_*) = \frac{x_*^2}{y_*^2(x_*^2 + \alpha^2)} > 0,$$
$$g_x(x_*, y_*, 0, \eta_*) = \frac{-ey_*^2}{A + y_*} < 0, \quad g_d(x_*, y_*, 0, \eta_*) = \frac{y_*^2}{d^2} > 0,$$

where

$$\eta_* = \left(\alpha^2, e, A, d\right) \left(\text{with} \quad d = \frac{y_* \left(A + y_*\right)}{A + y_* - e x_* y_*} \right).$$

It follows from [17] that E is a canard point.

For these cases of $E = E_1$ or $E = E_2$, we can define singular canard cycles with and without head as well as transitory canard (see Figure 8(a) and (d), (b) and (e) as well as (c) and (f)respectively). Such singular canard cycles can be parameterized by certain parameter.

Let (x_1, y_1) and (x_2, y_2) be the coordinates of the folded points E_1 and E_2. Moreover, let x_l, x_m, x_r be the x-coordinates of the points lying on the branches M_0^l, M_0^m and M_0^r respectively solved from $\varphi(x) = s$ with $s \in (0, s_0)$, where $s_0 = y_1 - y_2$ and $x_l(s) < x_m(s) < x_r(s)$.

Let $x_m(0) = x_r(0) = x_1$, $x_l(s_0) = x_m(s_0) = x_2$. Then the singular canard cycles shown in Figure 8(a) and (b) can be parameterized by

$$\Gamma_1(s) = \{(x, \varphi(x)) : x \in [x_l(s), x_m(s)]\} \cup \{(x, s) : x \in [x_l(s), x_m(s)]\}, \ s \in [0, s_0],$$

and the singular canard cycles in Figure 8(c) can be parameterized by

$$\Gamma_1(s) = \{(x, \varphi(x)) : x \in [x_l(y_2), x_m(2s_0 - s)]\} \cup (x, 2s_0 - s) : x \in [x_m(2s_0 - s), x_r(2s_0 - s)]$$

$$\cup \{(x, \varphi(x)) : x \in [x_2, x_r(2s_0 - s)]\} \cup \{(x, y_2) : x \in [x_l(y_2), x_2]\}, \ s \in [s_0, 2s_0].$$

The singular canard cycles shown in Figure 8(d), (e) and (f) denoted by $\Gamma_2(s)$ can be parameterized in a similar way, which are omitted here.

For sufficient small ε, if there exists a small amplitude limit cycle (Hopf cycle) growing into a family of canard cycles followed by a large amplitude relaxation oscillation, this phenomenon is called canard explosion if this transition is completed within an exponentially small range $O(\exp(-1/\varepsilon))$ of the control parameter (see Krupa and Szmolyan [16]). To investigate the birth of canard explosion, we need to use the canard theory developed by Krupa and Szmolyan [16].

Let us transfer system (3.3) to its standard slow-fast normal form. The first is the translation, $u = x - x_*, v = y - x_*$ and $d = d_* - \lambda$, where $d_* = d_1$, when $(x_*, y_*) = (x_1, y_1)$ (respectively $d_* = d_2$, when $(x_*, y_*) = (x_2, y_2)$), then system (3.3) can be rewritten as

$$\begin{aligned}
x' &= p_0 + p_1 u + p_2 \varepsilon + v \left(p_3 + p_4 u + p_5 v + O\left(|(u,v)|^2\right)\right) + u^2 \left(p_6 + p_7 u + O\left(u^2\right)\right) \\
&\quad + \varepsilon O(u, \lambda, v), \\
y' &= \varepsilon \left(q_0 + u \left(q_1 + q_2 v + O\left(v^2\right)\right) + \lambda \left(q_3 + q_4 \lambda + q_5 v + O\left(|(\lambda, v)|^2\right)\right)\right) \\
&\quad + v\varepsilon \left(q_6 + q_7 v + O\left(v^2\right)\right),
\end{aligned}$$

(4.1)

where

$$\begin{aligned}
p_0 &= -x_*(x_* - 1) - \frac{x_*^2}{y_* \left(\alpha^2 + x_*^2\right)}, \\
p1 &:= -\frac{2\alpha^4 x_* y_* + 4\alpha^2 x_*^3 y_* + 2x_*^5 y_* - \alpha^4 y_* - 2\alpha^2 x_*^2 y_* - x_*^4 y_* + 2\alpha^2 x_*}{y_* \left(\alpha^2 + x_*^2\right)^2}, \\
p_2 &= -\frac{x_* \left(-ed_* x_* y_* + A d_* - A y_* + d_* y_* - y_*^2\right)}{d_* \left(A + y_*\right)},
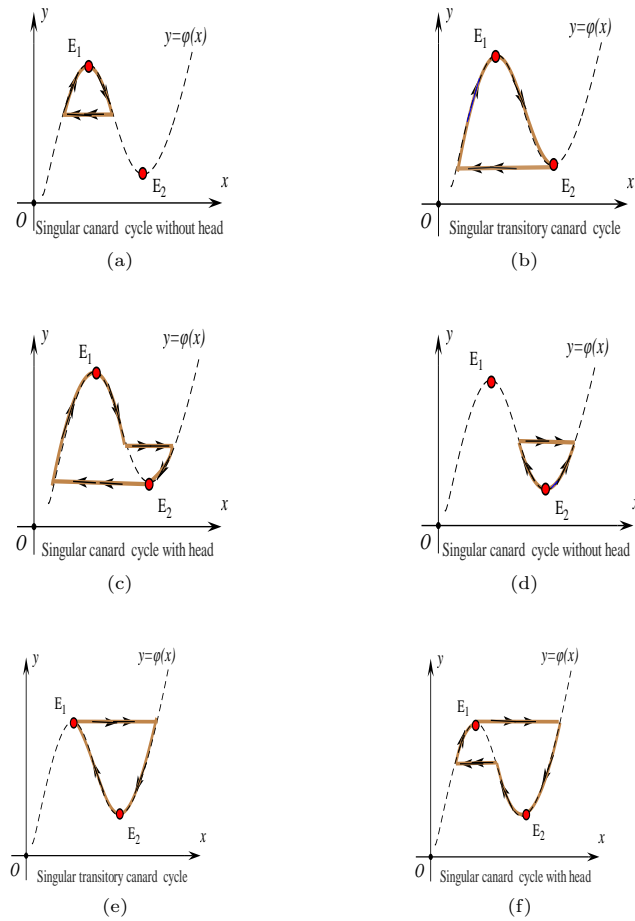\end{aligned}$$

Figure 8. (a) and (d): Singular canard cycles without head; (b) and (e): Transitory canards; (c) and (f): Singular canard cycles with head (see the brown curves).

$$p_3 = \frac{x_*^2}{y_*^2 \left(\alpha^2 + x_*^2\right)}, \quad p_4 = \frac{2x_*\alpha^2}{y_*^2 \left(\alpha^2 + x_*^2\right)^2}, \quad p_5 = -\frac{x_*^2}{y_*^3 \left(\alpha^2 + x_*^2\right)},$$

$$p_6 = -\frac{\alpha^6 y_* + 3\alpha^4 x_*^2 y_* + 3\alpha^2 x_*^4 y_* + x_*^6 y_* + \alpha^4 - 3\alpha^2 x_*^2}{y_* \left(\alpha^2 + x_*^2\right)^3},$$

$$p_7 = \frac{4x_*\alpha^2 \left(\alpha^2 - x_*^2\right)}{y_* \left(\alpha^2 + x_*^2\right)^4}$$

and

$$q_0 = \frac{y_* \left(-ed_*x_*y_* + Ad_* - Ay_* + d_*y_* - y_*^2\right)}{d_* \left(A + y_*\right)},$$

$$q_1 = -\frac{y_*^2 e}{A + y_*}, \quad q_2 = -\frac{ey_* \left(2A + y_*\right)}{\left(A + y_*\right)^2},$$

$$q_3 = -\frac{y_*^2}{d_*^2}, \quad q_4 = -\frac{y_*^2}{d_*^3}, \quad q_5 = -\frac{2y_*}{d_*^2},$$

$$q_6 = \frac{-2Aed_*x_*y_* - ed_*x_*y_*^2 + A^2 d_* - 2A^2 y_* + 2Ad_*y_* - 4Ay_*^2 + d_*y_*^2 - 2y_*^3}{d_* \left(A + y_*\right)^2},$$

$$q_7 = -\frac{A^2 ed_*x_* + A^3 + 3A^2 y_* + 3Ay_*^2 + y_*^3}{\left(A + y_*\right)^3 d_*}.$$

By using the fact that when the positive equilibrium E coincides with the fold points E_1 or E_2, it must be

$$d_* = \frac{y_* \left(A + y_*\right)}{A + y_* - ex_*y_*},$$

$$p\left(x_*\right) = 2x_*^3 - x_*^2 + \alpha^2 = 0,$$

$$y_* = \varphi\left(x_*\right) = \frac{x_*}{\left(x_*^2 + \alpha^2\right)\left(1 - x_*\right)}, \tag{4.2}$$

which means

$$p_0 = 0, \quad p_1 = 0, \quad p_2 = 0, \quad q_0 = 0. \tag{4.3}$$

Then, by the following rescaling on variables and parameters,

$$u \to p_6 \left(-p_3 q_1\right)^{-\frac{1}{2}} u, \quad v \to p_6 q_1^{-1} v, \quad \lambda \to -q_3 p_6 q_1^{-1} \left(-p_3 q_1\right)^{-\frac{1}{2}} \lambda, \quad \bar{s} \to \left(-p_3 q_1\right)^{\frac{1}{2}} \bar{s},$$

we get the normal form system as follows

$$\begin{aligned} \frac{du}{d\bar{s}} &= -vh_1 + u^2 h_2 + \varepsilon h_3, \\ \frac{dv}{d\bar{s}} &= \varepsilon \left(uh_4 - \lambda h_5 + vh_6\right) \end{aligned} \tag{4.4}$$

with

$$h_1 = 1 + p_4 p_6 p_3^{-1} \left(-p_3 q_1\right)^{-\frac{1}{2}} u + p_5 p_6 p_3^{-1} q_1^{-1} v + O\left(|(u,v)|^2\right),$$

$$h_2 = 1 + p_7 \left(-p_3 q_1\right)^{-\frac{1}{2}} u + O\left(u^2\right),$$

$$h_3 = O(u, v, \lambda),$$

$$h_4 = 1 + q_2 p_6 q_1^{-2} v + O(v^2),$$

$$h_5 = 1 + (-p_5 p_6 q_1^{-1} (-p_3 q_1)^{-\frac{1}{2}})\lambda + p_6 q_5 q_3^{-1} q_1^{-1} v + O\left(|(v,\lambda)|^2\right),$$

$$h_6 = q_6 (-p_3 q_1)^{\frac{1}{2}} + p_6 q_7 q_1^{-1} (-p_3 q_1)^{\frac{1}{2}} v + O\left(v^2\right).$$

Here, we have successfully transformed system (3.3) into (4.4), its normal form, in which the quantities defined in (3.12) of Krupa and Szmolyan [16] are now given respectively by

$$a_1 = \left.\frac{\partial h_3}{\partial u}\right|_O = 0,$$

$$a_2 = \left.\frac{\partial h_1}{\partial u}\right|_O = -\frac{2\alpha^2 \left(\alpha^6 y_* + 3\alpha^4 x_*^2 y_* + 3\alpha^2 x_*^4 y_* + x_*^6 y_* + \alpha^4 - 3\alpha^2 x_*^2\right)}{x_* y_* \left(\alpha^2 + x_*^2\right)^4 B},$$

$$a_3 = \left.\frac{\partial h_2}{\partial u}\right|_O = \frac{4x_* \alpha^2 \left(\alpha^2 - x_*^2\right)}{y_* \left(\alpha^2 + x_*^2\right)^4 B}, \quad a_4 = \left.\frac{\partial h_4}{\partial u}\right|_O = 0,$$

$$a_5 = h_6|_O$$

$$= \frac{B \left(-2Aed_* x_* y_* - ed_* x_* y_*^2 + A^2 d_* - 2A^2 y_* + 2Ad_* y_* - 4Ay_*^2 + d_* y_*^2 - 2y_*^3\right)}{d_* \left(A + y_*\right)^2},$$

where $B = \sqrt{\frac{x_*^2 e}{(\alpha^2 + x_*^2)(A + y_*)}}$ and $O = (0,0,0,0)$.

Accordingly, the quantity defined in (3.13) of Krupa and Szmolyan [16] turns out to be

$$\tilde{A}_* = -a_2 + 3a_3 - 2a_4 - 2a_5$$

$$= \frac{2\alpha^2 \left(\alpha^6 y_* + 3\alpha^4 x_*^2 y_* + 3\alpha^2 x_*^4 y_* + x_*^6 y_* + \alpha^4 - 3\alpha^2 x_*^2\right)}{x_* y_* \left(\alpha^2 + x_*^2\right)^4 B} + \frac{12x_* \alpha^2 \left(\alpha^2 - x_*^2\right)}{y_* \left(\alpha^2 + x_*^2\right)^4 B}$$

$$- \frac{2B \left(-2Aed_* x_* y_* - ed_* x_* y_*^2 + A^2 d_* - 2A^2 y_* + 2Ad_* y_* - 4Ay_*^2 + d_* y_*^2 - 2y_*^3\right)}{d_* \left(A + y_*\right)^2}.$$

$$(4.5)$$

Remark 4.2. We know that the sign of $\tilde{A}_*$ determines whether the Hopf bifurcation is supercritical or subcritical. Nevertheless, it is very difficult to determine the sign of $\tilde{A}_*$ due to its complexity, see (4.5). Numerical examples verify that all the three cases $\tilde{A}_* < 0, = 0, > 0$ are possible. For example, when $\varepsilon = 0.0005$, we have the follows.

(i_1) Setting $\alpha^2 = 0.01, e = 12, A = 3, d_1 = 50.3243$, one has $E_1(0.113781, 5.59525)$, $\tilde{A}_1 = -56.6611 < 0$.
Setting $\alpha^2 = 0.02, e = 10, A = 15, d_1 = 5.50104$, one has $E_1(0.175564, 4.19006)$, $\tilde{A}_1 = 0$.
Setting $\alpha^2 = 0.017, e = 7, A = 10, d_1 = 6.78313$, one has $E_1(0.157546, 4.47167)$, $\tilde{A}_1 = 4.34698 > 0$.

(i_2) Setting $\alpha^2 = 0.015, e = 15, A = 27, d_2 = 25.5821$, one has $E_2(0.465369, 3.75893)$, $\tilde{A}_2 = -0.775098 < 0$.
Setting $\alpha^2 = 0.024, e = 6, A = 8, d_2 = 3.23523$, one has $E_2(0.437228, 3.61075)$, $\tilde{A}_2 = 0$.
Setting $\alpha^2 = 0.003, e = 18, A = 32, d_2 = 172.940$, one has $E_2(0.493850, 3.95119)$, $\tilde{A}_2 = 0.908115 > 0$.

Here, it should be pointed out that the value of α is chosen to satisfy $0 < \alpha^2 < \frac{1}{27}$, e, A, d_1, d_2 are selected to be positive, and d_1, d_2 are accordingly determined by following the formula given in Remark 4.1.

So far, the singular Hopf bifurcation curve λ_{*H} and the maximal canard curve λ_{*c} are respectively

$$\lambda_{*H}(\sqrt{\varepsilon}) = -\left(\frac{a_1 + a_5}{2}\right)\varepsilon + O\left(\varepsilon^{\frac{3}{2}}\right)$$

and

$$\lambda_{*c}(\sqrt{\varepsilon}) = -\left(\frac{a_1 + a_5}{2} + \frac{1}{8}\tilde{A}_*\right)\varepsilon + O\left(\varepsilon^{\frac{3}{2}}\right).$$

After taking the translation as well as the rescaling on the parameter λ into account, the singular Hopf bifurcation curve λ_{*H} and the maximal canard curve d_{*c} expressed in terms of the original parameters of system (3.3) are

$$d_{*H}(\sqrt{\varepsilon}) = d_* + p_6 q_3 q_1^{-1}\left(-p_3 q_1\right)^{-\frac{1}{2}}\left(-\left(\frac{a_1 + a_5}{2}\right)\varepsilon + O\left(\varepsilon^{\frac{3}{2}}\right)\right) \qquad (4.6)$$

and

$$d_{*c}(\sqrt{\varepsilon}) = d_* + p_6 q_3 q_1^{-1}\left(-p_3 q_1\right)^{-\frac{1}{2}}\left(-\left(\frac{a_1 + a_5}{2} + \frac{1}{8}\tilde{A}_*\right)\varepsilon + O\left(\varepsilon^{\frac{3}{2}}\right)\right). \quad (4.7)$$

It is worthy noting again that the symbol $*$ stands for $1, 2$ corresponding to the cases of $E = E_1$ and $E = E_2$ respectively.

According to Theorems 3.1, 3.3 and 3.4 in [16], one obtains the following conclusions.

- There exist $\varepsilon_0 > 0$, $\sigma_0 > 0$ and the smooth curve $d_{*H}(\sqrt{\varepsilon})$ given in equation (4.6), which is defined in the region $(0, \varepsilon_0) \times (d_* - \sigma_0, \ d_* + \sigma_0)$ of the parameter plane (ε, d), such that system (3.3) has a unique positive equilibrium E, which is stable for $d < d_{*H}(\sqrt{\varepsilon})$ and unstable for $d > d_{*H}(\sqrt{\varepsilon})$. In addition, the Hopf bifurcation is non-degenerate if $\tilde{A}_* \neq 0$, and furthermore, it is supercritical for $\tilde{A}_* < 0$ and subcritical for $\tilde{A}_* > 0$, where $\tilde{A}_*$ is given by (4.5).

- When the equilibrium moves near the canard point $E = E_1$ and $\tilde{A}_1 < 0$, there is a smooth function (near d_1),

$$d_{1c}(\sqrt{\varepsilon}) = d_1 + p_6 q_3 q_1^{-1}\left(-p_3 q_1\right)^{-\frac{1}{2}}\left(-\left(\frac{a_1 + a_5}{2} + \frac{1}{8}\tilde{A}_1\right)\varepsilon + O\left(\varepsilon^{\frac{3}{2}}\right)\right),$$

along which, for ε sufficiently small there is a family of periodic orbits

$$s \to \left(d_1(s, \sqrt{\varepsilon}), \Gamma_1(s, \sqrt{\varepsilon})\right), \quad s \in (0, 2(y_1 - y_2)),$$

which are smooth in $(s, \sqrt{\varepsilon})$ and such that

(i_1) for $s \in (0, \varepsilon^v)$, the orbit $\Gamma_1(s, \sqrt{\varepsilon})$ is attracting and uniformly $O(\varepsilon^v)$ close to the canard point E_1 and $d_1(s, \sqrt{\varepsilon})$ is strictly increasing in s;

(i_2) for $s \in (2(y_1 - y_2) - \varepsilon^v, 2(y_1 - y_2))$, the orbit $d_1(s, \sqrt{\varepsilon})$ is a relaxation oscillation and $d_1(s, \sqrt{\varepsilon})$ is strictly increasing in s;

(i_3) for $s \in [\varepsilon^v, (2(y_1 - y_2) - \varepsilon^v]$,

$$\left| d_1(s, \sqrt{\varepsilon}) - d_{1c}(\sqrt{\varepsilon}) \right| \leqslant e^{-1/\varepsilon^{1-v}} and$$

(i_4) as $\varepsilon \to 0$, the family $\Gamma_1(s, \sqrt{\varepsilon})$ converges uniformly in Hausdorff distance to $\Gamma_1(s)$.

- When the equilibrium moves close to the canard point $E = E_2$ and $\tilde{A}_2 > 0$ holds, there exists another smooth function (near d_2),

$$d_{2c}(\sqrt{\varepsilon}) = d_2 + p_6 q_3 q_1^{-1} \left(-p_3 q_1 \right)^{-\frac{1}{2}} \left(-\left(\frac{a_1 + a_5}{2} + \frac{1}{8} \tilde{A}_2 \right) \varepsilon + O\left(\varepsilon^{\frac{3}{2}} \right) \right).$$

For ε sufficiently small and $\nu \in (0, 1)$, there exists a family of periodic orbits

$$s \to \left(d_2(s, \sqrt{\varepsilon}), \Gamma_2(s, \sqrt{\varepsilon}) \right), \quad s \in (0, 2(y_1 - y_2)),$$

which is smooth in $(s, \sqrt{\varepsilon})$, and such that

(i_1) for $s \in (0, \varepsilon^v)$, the orbit $\Gamma_2(s, \sqrt{\varepsilon})$ is repelling and uniformly $O(\varepsilon^v)$ close to the canard point E_2 and $d_2(s, \sqrt{\varepsilon})$ strictly decreasing in s;
(i_2) for $s \in (2(y_1 - y_2) - \varepsilon^v, 2(y_1 - y_2))$, the orbit $\Gamma_2(s, \sqrt{\varepsilon})$ is a relaxation oscillation and $d_2(s, \sqrt{\varepsilon})$ strictly increasing in s;
(i_3) for $s \in [\varepsilon^v, (2(y_1 - y_2) - \varepsilon^v]$,

$$\left| d_2(s, \sqrt{\varepsilon}) - d_{2c}(\sqrt{\varepsilon}) \right| \leqslant e^{-1/\varepsilon^{1-v}} and$$

(i_4) as $\varepsilon \to 0$, the family $\Gamma_2(s, \sqrt{\varepsilon})$ converges uniformly in Hausdorff distance to $\Gamma_2(s)$.

Set

$$d_{1s}(\sqrt{\mu}) = d_1\left(\varepsilon^\nu, \sqrt{\varepsilon} \right), d_{1r}(\sqrt{\varepsilon}) = d_1\left(2(y_1 - y_2) - \varepsilon^\nu, 2(y_1 - y_2) \right),$$
$$d_{2s}(\sqrt{\mu}) = d_2\left(\varepsilon^\nu, \sqrt{\varepsilon} \right), d_{2r}(\sqrt{\varepsilon}) = d_2\left(2(y_1 - y_2) - \varepsilon^\nu, 2(y_1 - y_2) \right),$$

where the subscripts s and r respectively stand for the small limit cycle and the relaxation oscillation.

With the analysis given above, when d increases from d_1 to d_{1s} we can conclude the following statements. First, there is a stable, small Hopf limit cycle, and it becomes a canard cycle, then with d increasing from d_{1s} to d_{1r}, the canard cycle continuously, quickly becomes a transitory canard cycle, a canard cycle with head and a stable relaxation oscillation. This process is called the first canard explosion of model (3.3). When the value of d is between d_{1r} and d_{2r}, the relaxation oscillation persists for a long term. As d increases from d_{2r} to d_{2s}, the canard cycle continuously becomes a canard cycle with head, a transitory canard cycle, and a small canard cycle without head from the relaxation oscillation continuously and quickly. This process is the second canard explosion occurring in model (3.3). Finally, when d increases from d_{2s} to d_2, the small canard cycle without head shrinks to a Hopf limit cycle such that periodic motions disappear there. Unlike the first canard explosion, the second canard explosion makes the relaxation oscillation disappear. Therefore, it is called inverse canard explosion.

Up to now, we have completed the proof of Theorem 4.1(B). In the next subsection, we turn to verify the theoretical predictions via numerical simulations.

4.3. Numerical simulation

Let $\alpha^2 = 0.003 < \frac{1}{27}$. Then, the associated critical curve $y = \varphi(x)$ has the maximal point $E_1(x_1, y_1) = (0.2403575621, 3.604904601)$ and the minimal point $E_2(x_2, y_2) = (0.4113537611, 3.507888534)$. Setting $A = 10$, $e = 16$, when $d = d_1 = 6.459985002$, the equilibrium E exactly coincides with E_1, and when $d = d_2 = 13.47592141$, the equilibrium E coincides with E_2.

Taking $\varepsilon = 0.0005$ and an arbitrarily initial point $(x_1 - 0.01, y_1 - 0.15)$, we obtain the whole dynamical process described in Theorem 4.2(B) by varying d from d_1 to d_2 increasingly (see Figure 9). In Figure 9, the magenta curve stands for the orbit of system (3.3) and the green dash one represents the critical curve. More precisely, the exact values of d in Figure 9 corresponding Figure 9(a)-(l) are respectively as follows

$(a) : d_1 + 0.01, \quad (b) : d_1 + 0.01425925, \quad (c) : d_1 + 0.01425929250508,$

$(d) : d_1 + 0.0142595, \quad (e) : d_1 + 0.01433, \quad (f) : d_1 + 0.55, \quad (g) : d_2 - 5,$

$(h) : d_2 - 0.09, \quad (i) : d_2 - 0.067, \quad (j) : d_2 - 0.0654219,$

$(k) : d_2 - 0.065402, \quad (l) : d_2 - 0.000001.$

From Figure 9, we can see that, when d increases near d_1, the orbit of system (3.3) begins from a small limit cycle (see Figure 9(a)) to a canard cycle without head (see Figure 9(b)), and then a transition canard (see Figure 9(c)), a canard cycle with head (see Figure 9(d) and (e)) and a relaxation oscillation cycle (see Figure 9 (f)). This process is the first canard explosion.

As d continually increases, the relaxation oscillation cycle lasts for a rather large range of parameter values, i.e., $d \in (d_1, d_2)$. Until d reaches near d_2, the orbit goes around the canard point E_2 several times (see Figure 9(g)) and then ultimately becomes a canard cycle with head (see Figure 9(h) and (i)), a transition canard cycles (see Figure 9(j)), a canard cycle without head (see Figure 9(k)) and finally a small limit cycle (see Figure 9(l)). This process is the second canard explosion, i.e., the inverse canard explosion.

Now, it can be concluded that all the theoretical analysis has been verified by numerical simulations.

5. Conclusions

In the current work, we explore the birth and the annihilation of canard explosions as well as relaxation oscillations in a two-dimensional singular perturbation spruce-budworm model by using GSPT and canard theory. Two critical values of the breaking parameter (expressed in terms of the original parameters of the model) are determined. Biologically, this means that periodic motions with budworm outbreaks can exist only within this parameter region under the circumstance which the intrinsic growth rates of the budworm and the spruce are of different orders. When the parameters are in this region, long term slow accumulation of the budworm will inevitably lead to a rapid outbreak. All these theoretical predictions including the birth and the annihilation of canard explosions and relaxation oscillations are captured and visualized by numerical simulations.

In this article, we apply GSPT and canard theory to detect the occurrence of canard explosion, inverse canard explosion and relaxation oscillations. GSPT and
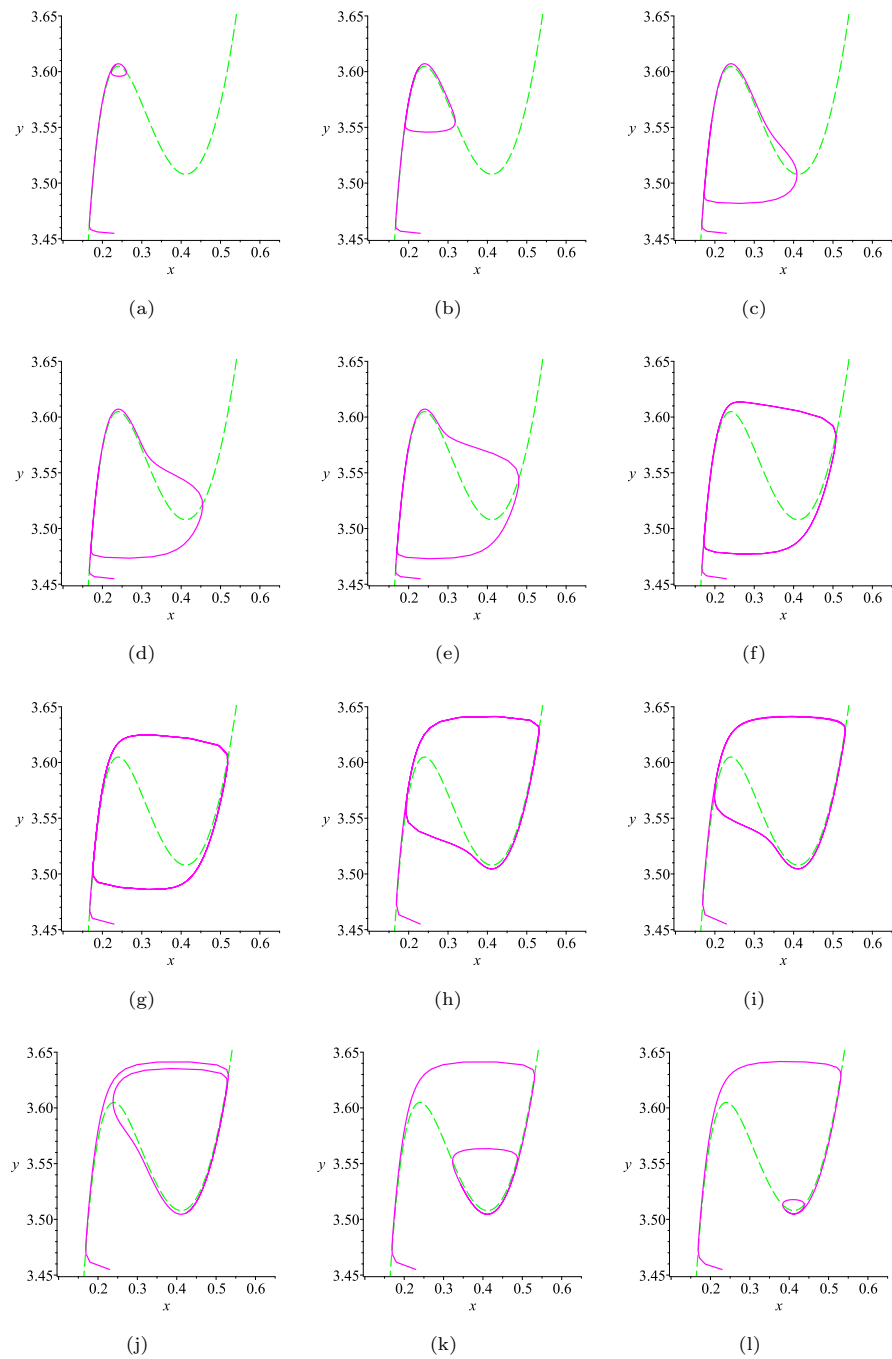
Figure 9. The continuously dynamical process of canard explosion and inverse canard explosion when the d varies increasingly from d_1 to d_2.

canard theory are geometric approaches. In these methods, after transforming the model under consideration into its associated normal form, one can easily capture the breaking parameter, which governs the birth as well as the annihilation of canard explosions and relaxation oscillations. Accordingly, the mechanisms governing the birth and the termination of canard explosions and relaxation oscillations can be seen more evident by these methods.

Acknowledgements

References

[1] P. Aguirre, J. D. Flores and E. González-Olivares, *Bifurcations and global dynamics in a predator-prey model with a strong Allee effect on the prey, and a ratio-dependent functional response*, Nonlinear Analysis: Real World Applications, 2014, 16, 235–249.

[2] A. Algaba, K. W. Chung, B. Qin and A. Rodríguez-Luis, *Analytical approximation of the canard explosion in a van der Pol system with the nonlinear time transformation method*, Physica D: Nonlinear Phenomena, 2020, 406, Article ID 132384, 9 pages.

[3] A. Atabaigi and A. Barati, *Relaxation oscillations and canard explosion in a predator-prey system of Holling and Leslie types*, Nonlinear Analysis: Real World Applications, 2017, 36, 139–153.

[4] E. Benoit, J. L. Callot, F. Diener and M. Diener, *Chasse au canard*, Collectanea Mathematica, 1981, 32(2), 77–97.

[5] S. Chen, J. Duan and J. Li, *Double canard cycles in singularly perturbed planar systems*, Nonlinear Dynamics, 2021, 105(4), 3715–3730.

[6] S. Chen, J. Duan and J. Li, *Dynamics of the Tyson-Hong-Thron-Novak circadian oscillator model*, Physica D: Nonlinear Phenomena, 2021, 420, Article ID 132869, 16 pages.

[7] X. Chen and X. Zhang, *Dynamics of the predator-prey model with the Sigmoid functional response*, Studies in Applied Mathematics, 2021, 147(1), 300–318.

[8] W. Ding and W. Huang, *Global Dynamics of a Predator-Prey Model with General Holling Type Functional Responses*, Journal of Dynamics and Differential Equations, 2020, 32(2), 965–978.

[9] F. Dumortier, *Techniques in the Theory of Local Bifurcations: Blow-Up, Normal Forms, Nilpotent Bifurcations, Singular Perturbations*, Bifurcations and Periodic Orbits of Vector Fields, Springer, Dordrecht, 1993.

[10] M. Falconi, M. Huenchucona and C. Vidal, *Stability and global dynamic of a stage-structured predator-prey model with group defense mechanism of the prey*, Applied Mathematics and Computation, 2015, 270, 47–61.

[11] N. Fenichel, *Geometric singular perturbation theory for ordinary differential equations*, Journal of Differential Equations, 1979, 31(1), 53–98.

[12] R. A. Fleming and C. A. Shoemaker, *Evaluating Models for Spruce Budworm-Forest Management: Comparing Output with Regional Field Data*, Ecological Applications: Ecological Society of America, 1992, 2(4), 460–477.

[13] G. Hek, *Geometric singular perturbation theory in biological practice*, Journal of Mathematical Biology , 2010, 60(3), 347–386.

[14] C. Jones, *Geometric Singular Perturbation Theory, in Dynamical Systems*, Springer, Berlin, 1995.

[15] M. H. Kabir, *Reaction-diffusion modeling of the spread of spruce budworm in boreal ecosystem*, Journal of Applied Mathematics and Computing, 2021, 66(1–2), 203–219.

[16] M. Krupa and P. Szmolyan, *Relaxation Oscillation and Canard Explosion*, Journal of Differential Equations, 2001, 174(2), 312–368.

[17] M. Krupa and P. Szmolyan, *Extending geometric singular perturbation theory to nonhyperbolic points-fold and canard points in two dimensions*, SIAM Journal on Mathematical Analysis, 2001, 33(2), 286–314.

[18] C. Li, J. Li, Z. Ma and H. Zhu, *Canard phenomenon for an SIS epidemic model with nonlinear incidence*, Journal of Mathematical Analysis and Applications, 2014, 420(2), 987–1004.

[19] C. Li and H. Zhu, *Canard cycles for predator-prey systems with Holling types of functional response*, Journal of Differential Equations, 2013, 254(2), 879–910.

[20] W. Liu, *Geometric Singular Perturbations for Multiple Turning Points: Invariant Manifolds and Exchange Lemmas*, Journal of Dynamics and Differential Equations, 2006, 18(3), 667–691.

[21] N. G. Lloyd, *Theory of Limit Cycles*, Bulletin of the London Mathematical Society, 1988, 20(2), 183–184.

[22] D. Ludwig, D. Jones and C. Holling, *Qualitative Analysis of Insect Outbreak Systems: The Spruce Budworm and Forest*, Journal of Animal Ecology, 1978, 47(1), 315–332.

[23] P. De Maesschalck, G. Kiss and A. Kovacs, *Relaxation oscillations and canards of a regulated two-gene model*, Journal of Mathematical Analysis and Applications, 2021, 502(1), Article ID 125144, 18 pages.

[24] R. M. May, *Thresholds and breakpoints in ecosystems with a multiplicity of stable states*, Nature, 1977, 269(5628), 471–477.

[25] J. Moehlis, *Canards in a Surface Oxidation Reaction*, Journal of Nonlinear Science, 2002, 12(4), 319–345.

[26] H. Peng and X. Zhang, *The Dynamics of Stochastic Predator-prey Models with Non-constant Mortality Rate and General Nonlinear Functional Response*, Journal of Nonlinear Modeling and Analysis, 2020, 2(4), 495–511.

[27] B. Qin, K. W. Chung, A. Algaba, et al., *Asymptotic expansions for a degenerate canard explosion*, Physica D: Nonlinear Phenomena, 2021, 418, Article ID 132841, 12 pages.

[28] A. Rasmussen, J. Wyller and J. O. Vik, *Relaxation oscillations in spruce-budworm interactions*, Nonlinear Analysis: Real World Applications, 2011, 12(1), 304–319.

[29] H. G. Rotstein, S. Coombes and A. M. Gheorghe, *Canard-Like Explosion of Limit Cycles in Two-Dimensional Piecewise-Linear Models of FitzHugh-Nagumo Type*, SIAM Journal on Applied Dynamical Systems, 2012, 11(1), 135–180.

[30] T. Royama, W. E. MacKinnon and E. G. Kettela, et al., *Analysis of Spruce Budworm Outbreak Cycles in New Brunswick, Canada, Since 1952*, Ecology, 2005, 86(5), 1212–1224.

[31] T. Saha, P. J. Pal and M. Banerjee, *Relaxation oscillation and canard explosion in a slow-fast predator-prey model with Beddington–DeAngelis functional response*, Nonlinear Dynamics, 2021, 103(1), 1195–1217.

[32] J. Shen, *Canard limit cycles and global dynamics in a singularly perturbed predator-prey system with non-monotonic functional response*, Nonlinear Analysis: Real World Applications, 2016, 31, 146–165.

[33] J. Song, *Qualitative Analysis of a Predator-prey System with Ratio-dependent and Modified Leslie-Gower Functional Response*, Journal of Nonlinear Modeling and Analysis, 2020, 2(3), 317–332.

[34] Y. Tai and Z. Zhang, *Relaxation oscillations in a Spruce-Budworm interaction model with Holling's type II functional response*, Discrete and Continuous Dynamical Systems. Series B., 2021, 26(4), 2173–2199.

[35] C. Wang and X. Zhang, *Canards, heteroclinic and homoclinic orbits for a slow-fast predator-prey model of generalized Holling type III*, Journal of Differential Equations, 2019, 267(6), 3397–3441.

[36] D. W. Williams and A. M. Liebhold, *Spatial Synchrony of Spruce Budworm Outbreaks in Eastern North America*, Ecology, 2000, 81(10), 2753–2766.

[37] C. Xu, S. Yuan and T. Zhang, *Global dynamics of a predator-prey model with defense mechanism for prey*, Applied Mathematics Letters, 2016, 62, 42–48.

[38] L. Zhang and J. Zhang, *Stability and Hopf Bifurcation Analysis on a Spruce-Budworm Model with Delay*, Journal of Applied Analysis and Computation, 2020, 10(6), 2711–2721.

[39] T. Zhang, T. Xu, J. Wang and Z. Jiang, *Homoclinic Cycle and Homoclinic Bifurcations of a Predator-prey Model with Impulsive State Feedback Control*, Journal of Nonlinear Modeling and Analysis, 2020, 2(2), 227–240.